10

Hydrodynamic Controls of Anoxia in Shallow Lakes

Paul W. Jewell

The accumulation and preservation of organic carbon in sediments is enhanced by anoxia in the overlying water column. The causes of anoxia in shallow (< 100 m deep) lakes have been analyzed with a turbulence closure fluid dynamic model coupled to a simple, three-component geochemical model which utilizes Michaelis-Menten growth kinetics. The model demonstrates that anoxia is enhanced by high nutrient concentrations and that lakes of intermediate depth are more likely to have anoxic water. Turbulent shear energy production (resulting from surface wind stress) and buoyancy energy production (resulting from surface heat flux) can cause subtle changes in surface nutrient concentration and therefore photosynthesis. The model successfully reproduces seasonal time-depth data sets of temperature and oxygen in Esthwaite Water, a eutrophic lake in the English Lakes district, and Gem Lake, an oligotrophic lake in the Sierra Nevada. The model is less successful in predicting particulate organic carbon concentrations, in large part due to simplifications that are inherent in the model development. Preliminary comparison of generalized model output with paleolimnological reconstruction of open basin lacustrine sediments is encouraging.

The production, accumulation, and preservation of organic carbon in the sedimentary record is strongly dependent on the geochemistry and circulation of the overlying water column. The vertical movement of water transfers nutrients to surface water where they enhance photosynthesis and hence organic carbon production. Vigorous vertical water exchange also keeps deep water ventilated, thereby retarding the preservation and accumulation of organic carbon.

The oxygen content of water has long been recognized as a key variable in the carbon cycling of the earth's surface water. Oxygen, nitrate, sulfate, and other oxidants convert organic carbon into more soluble inorganic carbon. Depletion of oxygen significantly enhances the amount of organic carbon preserved in sediments (Blatt, Middleton, and Murray 1980; Emerson 1985). The precise chemical and physical conditions that cause anoxia have not, however,

been clearly established. Previous studies have focused on two primary factors: (1) surface productivity and the associated flux of organic carbon to the sediment-water interface and (2) the residence time of deep water. Note that in this discussion, high organic carbon *flux* does not imply high organic carbon *accumulation* or vice versa. High organic carbon accumulation can occur in oxygenated water and is a function of organic carbon flux and sedimentation rate as well as oxygen content of the water (Emerson 1985).

Anoxic settings have been broadly categorized into four types: (1) lakes whose bottom waters are anoxic as the result of water column stratification; (2) silled marine basins in which freshwater influx (either rainfall or river inflow) exceeds evaporation; (3) oceanic upwelling zones where deep, nutrient-rich water flows to the surface adjacent to a continental land mass; and (4) open ocean anoxia, which typically develops at middepths (200–1000 m) at the edges of some ocean basins (Demaison and Moore 1980). Various models of oxygen cycling and anoxia have been made for each of these four settings. A brief description of some of these models within the Demaison and Moore classification is given below. I then give a detailed discussion of a new model that has been successfully applied to one particular anoxic setting—shallow lakes.

Previous Numerical Models of Anoxia

Numerical models of dissolved oxygen concentrations are desirable for several reasons. Continuous spatial and temporal analytical measurements of oxygen are often impossible. On the other hand, numerical models that have been carefully verified by observational data provide a continuous representation of the modeling domain. Prognostic dissolved oxygen calculations are also important to engineers and public officials. For instance, dissolved hydrogen sulfide (a common component of anoxic water) is very corrosive to hydroelectric turbines in dams. Anoxic bottom water in reservoirs can therefore have a direct bearing on the economics of hydroelectric projects.

Quantitative models of anoxia can be broadly classified into two endmembers: box models and continuum models (figure 10.1). Box models assume uniform properties for a given domain (e.g., the deep water or surface water of ocean basins). Mass transfer between boxes is expressed as a series of mass balances and exchange rates. Changing a given property in one box or the exchange rate between boxes causes a response in the entire model. Box models are attractive because the computational effort is not burdensome as long as the numbers of boxes and parameters stay relatively small. Furthermore, box models give a clear picture of the cause and effect of changing variables. Box models have the disadvantage of being spatially discontinuous, with the result that many portions of the modeling domain cannot be studied in detail.

Continuum models, on the other hand, solve a differential equation for each quantity that influences the modeling domain. Each differential equation consists of accumulation, advection, diffusion, source, and/or sink terms for the variable being considered (figure 10.1). The quantity expressed by the differential equation varies continuously in space and time. In theory, a continuum model is simply a box model with an infinite number of "boxes." Continuum models have the advantage of showing the subtle and/or continuous changes of a property over the entire modeling domain. The disadvantage of continuum models is the complex solution of realistic problems (generally by some form of numerical method). This disadvantage becomes particularly acute for the 2- and 3-dimensional models that are often necessary to realistically represent a domain.

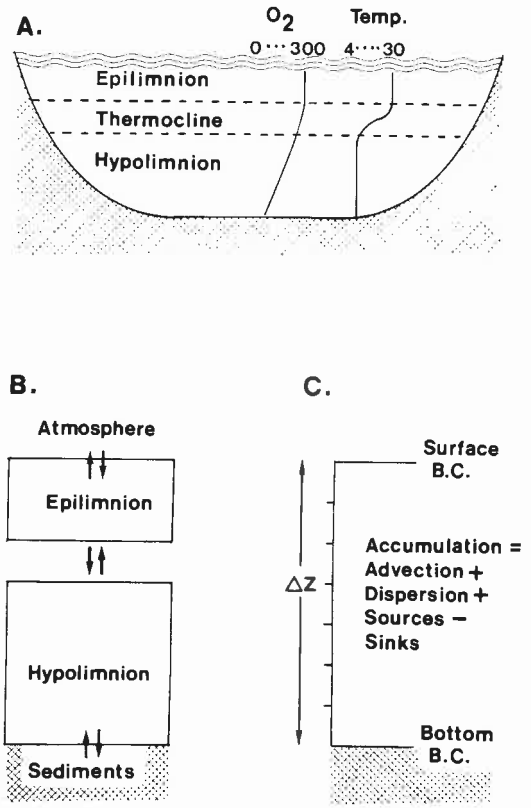

Figure 10.1. A. Idealized diagram of a lake showing the relationship between temperature (°C) and dissolved oxygen (μmole/L) in the epilimnion, thermocline, and hypolimnion. B. Diagrammatic box model of an idealized lake. C. Contiuum model of an idealized lake. The modeling domain is broken into Δz length segments in which a differential equation is solved for each variable.

Both box and continuum models have been effectively applied to marine and nonmarine anoxic regimes. Many early models were prompted by the desire of environmental engineers to predict the rate of eutrophication in lakes and reservoirs. Typically, these models treat different portions of the water column (e.g., the hypolimnion and epilimnion) as "continuous stirred tank reactors" (CSTR) (Snodgrass and O'Melia 1975; Higgins and Kim 1982; Gachter and Imboden 1985). CSTR models are essentially box models with a time derivative for each variable. For reservoirs and lakes in which the CSTR representation is appropriate, these models predict dissolved oxygen quite well. A frequent disadvantage of CSTR models is the large number of empirical constants that must be determined for each modeling problem (e.g., Snodgrass and O'Melia 1975:943–944).

Open ocean anoxia has been modeled from both box and continuum model perspectives. Southam and Peterson (1985) describe a COP (carbon-oxygen-phosphate) continuum model that represents the vertical distribution of chemical components over 0–4 km depths of the open ocean. The model is used to show that deep sea oxygen profiles can change dramatically over several hundred years in response to changes in mixed layer nutrient concentrations. These time scales are consistent with the time rate of change in atmospheric pressure of carbon dioxide (pCO_2) recorded in ice cores.

Shaffer (1989) uses a continuum model to study the relationships among oxygen, nitrogen, phosphorous, and sulfur in the ocean. The model uses simple physics to predict complex biogeochemical interactions. Model results show that anoxia in ocean basins is most likely when biological productivity is phosphorous limited and there is no phosphorite formation on the sea floor. Under other conditions (i.e., nitrogen limitation of productivity), oceanwide anoxia is difficult to maintain over geological timescales.

Multiple box models have been used to examine the causes of anoxia over whole ocean basins (Sarmiento, Herbert, and Toggweiler 1988a). These studies demonstrate that anoxia is not simply a function of long deep water residence time (which implies slow ocean circulation) or high surface productivity. Rather, oceanwide anoxia is critically dependent on the ratio of oxygen to reduced nutrients in areas of deep water formation. This ocean basin box model has been extended to the prediction of anoxia in the Mediterranean Sea (Sarmiento, Herbert, and Toggweiler 1988b). In this study, the Eastern and Western Mediterranean are treated as separate silled basins. The present exchange of water between the Eastern and Western Mediterranean prevents anoxia from occurring in either basin. In the geologic past, freshening of water in the Eastern Mediterranean reversed the exchange between these two basins. Under these conditions, anoxia developed in the Eastern Mediterranean but not in the Western Mediterranean.

Present Study

This paper presents a new type of continuum anoxia model. The model is well suited for studying anoxia that develops over relatively short time scales (the order of one year or less) in shallow water (less than 100 m depth). The present study is applied only to 1-dimensional (vertical) domains. Although the model requires moderate computing resources, it is capable of revealing many processes in the water column that are difficult or impossible to measure analytically.

One drawback of previous continuum anoxia models has been their inability to predict, a priori, the vertical mixing coefficient, eddy diffusivity. Eddy diffusivities are usually established on the basis of chemical tracer studies or a knowledge of the general physical setting of the modeling domain. This approach has proven satisfactory for studies in a relatively static water column where temporal variations of eddy diffusivity are small. In settings characterized by rapidly changing physical forcings, such as estuaries or the seasonal stratification and overturning in lakes, eddy diffusivities change many orders of magnitude in a short time. Even relatively static water columns have highly variable eddy diffusivities. For instance, empirical measurements of lake eddy diffusivities range from 10^{-5} to 10^{-9} m^2/s (Quay et al. 1980).

An alternative to using empirically derived eddy diffusivities involves computation of these terms from characteristics of the flow field itself. This approach parameterizes eddy diffusivity and eddy viscosity in terms of turbulent kinetic energy per unit mass. Solving for turbulent kinetic energy necessitates some sort of closure scheme, wherein both mean and turbulent variables are solved. The second-order turbulence closure scheme outlined by Mellor and Yamada (1974, 1982) has been successfully applied to a variety of settings in the ocean, including studies of the marine thermocline (Mellor and Durbin 1975), the marine bottom boundary layer (Weatherly and Martin 1978), and coastal estuaries (Oey, Mellor, and Hires 1985).

In the Mellor-Yamada model, the time rate of change of turbulent kinetic energy consists of shear energy production, buoyancy energy production, and a dissipation term. Shear and buoyancy energy production of turbulence are critical to understanding oxygen transport in natural waters (figure 10.2). High winds enhance shear production, which in turn causes oxygen produced in the photic zone to diffuse to deeper water levels. Surface heating, on the other hand, causes negative buoyancy production, thereby retarding the mixing of oxygenated surface water with deeper water. A viable anoxia model must therefore consider the competing effects of shear and buoyancy production (i.e., wind stress and surface heat flux).

The present study represents a first attempt to couple the turbulence closure model of Mellor and Yamada to a simple ecosystem model. The goals of the

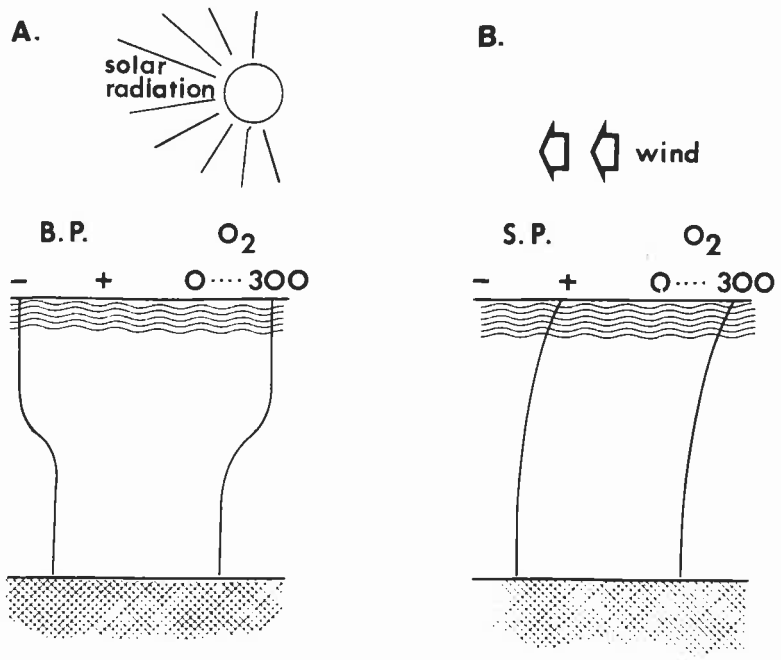

Figure 10.2. A. Relationship between dissolved oxygen (μmole/L) and buoyancy energy production (BP) during solar heating. Warm water tends to stratify the water column, cutting off the supply of O_2 to the underlying water. B. Relationship between dissolved oxygen (μmole/L) and shear energy production (SP) during a period of strong wind. Wind causes mixing, which fluxes O_2 to the deep water.

study are (1) to determine whether the model can accurately reproduce detailed geochemical data sets (specifically, dissolved oxygen and nutrients) in lakes and (2) to develop the theoretical framework whereby anoxia can be predicted from physical forcings such as wind and heat flux. Surface temperature and synoptic wind speed data sets are often readily available near lakes. On the other hand, measuring detailed physical and chemical properties over an entire water column on a continuing basis is a formidable analytical task. It is hoped that models such as the one described here can eventually alleviate some of the need for continuous field measurements in surface waters.

A variety of ecological models has been proposed to describe the distribution of nutrients and living organisms in natural waters (e.g., Walsh 1975; Jamart et al. 1977; Wroblewski 1977; Kremer and Nixon 1978; Hoffman and Ambler 1988; Hoffman 1988). These models all use varients of Michaelis-Menten kinetics to relate nutrient uptake to phytoplankton growth and have been reasonably successful in their reproduction of field data.

For this study, a simple three-component chemical model consisting of dissolved oxygen (O_2), dissolved phosphate (PO_4), and particulate organic carbon (POC) was used. The model is similar to other simple oxygen models (e.g., the COP model of Southam and Peterson 1985). The simple geochemical model

allows examination of the critical physical and chemical variables that control anoxia with reliance on a minimum of empirical constants. Details of the physical and chemical model are given in appendix 10.1.

Lakes were chosen for this initial study because much of the physical, chemical, and biological dynamics of lakes can be represented by a 1-dimensional model. The 1-dimensional model described here is now being extended to 2- and 3-dimensional models. It is hoped that these more sophisticated models will allow examination of the details of anoxic processes in silled basins, coastal upwelling zones, and other modeling domains of interest.

Idealized Lake Models

The model described in appendix 10.1 has been used to examine the physical and biological parameters that lead to lake anoxia. In the following discussion, an idealized model run over a single season is described. The idealized model permits detailed examination of energy balances, mixing, and surface productivity in a typical lake. Sensitivity analyses are used to examine the effect of lake depth and nutrient concentration on the development of anoxia. The sensitivity analyses are simply meant to highlight variables that are most critical to the development of lake anoxia. Absolute values of these variables should not be extrapolated from this example owing to the idealized nature of the model.

For the idealized model, an isothermal water column of 6°C was the initial temperature condition. Dissolved PO_4 was uniformly distributed throughout a 15-m-deep water column. Initial PO_4 was 2 μmole/L. A small amount of POC (0.2 μmole/L) throughout the water column was assumed to represent the seed phytoplankton. Oxygen was set equal to 100% of saturation throughout the water column. The water column was gradually stratified by increasing surface temperature to 19°C as a sine function over 125 days. The surface temperature was then decreased to 6°C over an additional 125 days. Overturn usually homogenized the water column at a temperature of about 8°C (figure 10.3A). The model was not run for an entire year, owing to complications of modeling an ice-covered lake. Wind stress was modeled as a daily sine wave with maximum value of 0.2 dynes/cm^2. Additional lake parameters are given in table 10.1. The idealized lake run parameters closely correspond to those of Esthwaite Water, the eutrophic lake described in more detail below.

Representative Model Run

The influence of physical parameters on POC and dissolved O_2 can be seen in figure 10.3. Eddy diffusivity, K_h, is relatively high in the epilimnion (10^{-3}m^2/s) but approaches molecular values (10^{-6} — 10^{-7} m^2/s) in the hypolimnion (figure

Table 10.1
Physical and biological parameters used in numerical models. Numbers in parentheses refer to values used in ideal model runs

Parameter	Symbol	Value	Notes
Molecular viscosity	ν_m	$(2.4 \times 10^{-7}) \times 10^{248.37/(T+133.15)}$ m^2s^{-1}	CRC 1977 *Handbook of Chemistry and Physics*
Molecular thermal diffusivity	ν_t	$(1.33 + .004 \times T) \times 10^{-7} m^2s^{-1}$	Emperical derivation of Batchelor (1967, appendix A)
Molecular oxygen diffusivity	ν_c, O_2	$1.7 \times 10^{-9} m^2s^{-1}$	Broeker and Peng (1982)
Molecular phosphate diffusivity	ν_c, PO_4	$6.0 \times 10^{-10} m^2s^{-1}$	Li and Gregory (1974)
Phytoplankton settling velocity	w_s	0.2 — 2.0 m d^{-1} (1.0 m d^{-1})	Smayda (1970)
Light half saturation constant	I_k	.0004 ly s^{-1} (green algae)	Parsons, Takahashi, and Hargrave (1984)
		.0011 ly s^{-1} (diatoms)	Parsons, Takahashi, and Hargrave (1984)
		.0027 ly s^{-1} (dinoflagellates)	Parsons, Takahashi, and Hargrave (1984)
		(.002 ly s^{-1})	
Nitrate half saturation constant	K_s, NO_3	.007 — .05 μmole/L (oceanic plankton)	Epply, Rogers, and McCarthy (1969)
		.03 — .36 μmole/L (neritic diatoms)	Epply, Rogers, and McCarthy (1969)
		.007 — .74 μmole/L (neritic flagellates)	Epply, Rogers, and McCarthy (1969)
Phosphate half saturation constant	K_s, PO_4	.0025-.000025 μmole/L (.001 μmole/L	Hanton (1969)
Oxygen half saturation constant	K_s, O_2	100 μmole/L	
Organic carbon regeneration rate	R_{max}	$5.7 \times 10^{-7} s^{-1}$	Westrich and Berner (1984)

10.3B). In late August and September, the deepening of the thermocline results in enhanced diffusivity ($K_h = 3 \times 10^{-3}$ m^2/s) through much of the water column.

An increase in surface POC occurs in late April (figure 10.3C). By June and July, surface POC declines significantly. After the surface temperature reaches a maximum in July, surface productivity and POC steadily increase. This increase is the result of deep water nutrients being mixed back into the photic zone by increasing eddy diffusivity (figure 10.3B). Maximum POC is reached when water column overturn mixes deep water back to the surface. Oxygen is gradually

depleted from the hypolimnion after the onset of thermal stratification (figure 10.3D). Bottom water anoxia (< 5 μmole/L) appears in late July and persists until the lake overturn in November.

The idealized model run shows the influence that shear and buoyancy energy production have on surface nutrients and hence POC production (figure 10.4). The shear energy production rate is at a maximum during the spring and then steadily decreases. By late August shear production is approximately 50% of its springtime value. Following this seasonal minimum, shear production steadily but irregularly increases until lake overturn. The decrease in shear production during stratification is caused by the inability of energy produced at the surface to be transmitted through the thermocline. Buoyancy energy production is antithetic to shear production (figure 10.4). Buoyancy production is negative throughout the period of thermal stratification but becomes positive once thermal overturn has passed. Note that the absolute amount of shear production (resulting from wind stress input) is more than an order of magnitude

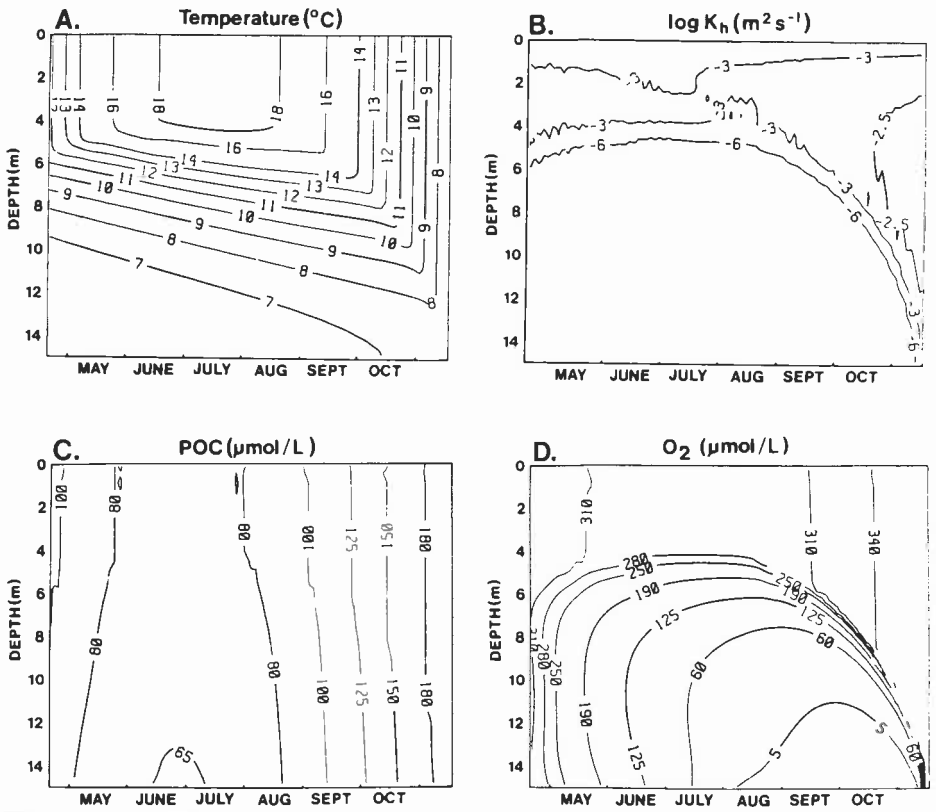

Figure 10.3. Time-versus-depth profiles for selected variables of the idealized model run. A. Temperature. B. Eddy diffusivity K_h. C. Particulate organic carbon. D. Dissolved oxygen.

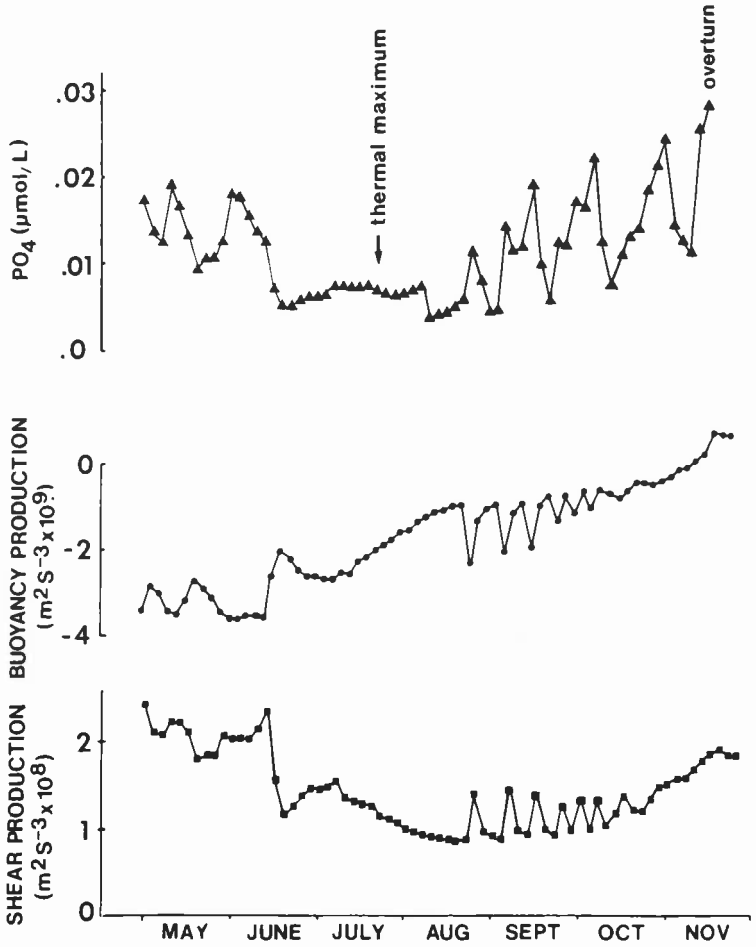

Figure 10.4. Seasonal variation of total photic zone phosphorus, average water column buoyancy production, and average water column shear production.

greater than buoyancy production (which results from surface heat flux). The irregular pattern of shear and buoyancy production reflects the fact that the model never achieves steady state. This is probably due to the continuously varying surface wind stress and heat flux boundary conditions (appendix 10.1, equation 15 and 17). Energy production irregularity is particularly pronounced following the thermal maximum (figure 10.4).

The influence of the combined energy production on surface nutrients and therefore photosynthesis is reflected in a plot of vertically integrated photic zone PO_4 versus time (figure 10.4). The photic zone is here defined as that portion of the water column in which photosynthesis exceeds respiration. The dropoff in photic zone PO_4 during the first month of the model run is caused by the spring uptake of POC (figure 10.3C). By late spring, photosynthesis has

effectively exhausted photic zone nutrients. By August, however, photic zone PO_4 begins to rise as a result of increased water column energy (i.e., the combined effect of buoyancy and shear production). In other words, when surface water passes the thermal maximum, deep water nutrients begin to be mixed back into the photic zone as the result of enhanced buoyancy and shear production and, therefore, eddy diffusivity. This effect is extremely subtle. Model phosphorous concentrations increase only slightly (less than 5×10^{-3} μmole/L) as a result of the change. Such small concentrations are well below the detection limit of routine water analyses, and therefore this effect has probably gone unnoticed in previous field studies of lakes.

Influence of Nutrient Concentration and Lake Depth

The total nutrient concentration of a lake has long been recognized as a key variable in determining the oxygen concentration of the bottom water (e.g., Gachter and Imboden 1985). The model presented here reconfirms this. A series of idealized model runs was conducted in which only initial PO_4 was changed. Low initial PO_4 (the order of 0.1 μmole/L) causes little change in bottom water anoxia (figure 10.5A). Concentrations an order of magnitude larger are necessary to bring about complete bottom water anoxia. Once again, caution should be used in extrapolating these results beyond the characteristics of this idealized lake (table 10.1).

Since model PO_4 (particulate plus dissolved) remains constant (appendix 10.1), the model cannot evaluate the effect of "PO_4 loading," i.e., the yearly influx of nutrients into the lake. PO_4 loading is considered a key variable in determining whether a lake will become eutrophic as the result of anthropogenic inputs (Vollenweider 1975). This study simply addresses the seasonal changes in PO_4 and O_2 without considering how longer term nutrient changes may cause anoxia.

Lake depth plays a critical role in determining the oxygen level of lake bottom water (figure 10.5B). Lake depth reflects total water volume and, hence, is a measure of the lake's chemical buffering capacity. In the specific case of seasonal anoxia, large, deep lakes that become oxygenated during spring overturn have the capacity to oxidize large amounts of organic carbon that sink out of the photic zone.

The ability of deep lakes to oxidize large amounts of organic matter has been recognized for many years. What is less obvious from previous studies is the ability of shallow lakes to remain oxygenated under the same conditions that cause somewhat deeper lakes to go anoxic (figure 10.5B). This is the result of wind-induced turbulence, which can mix oxygen to the bottom of shallow lakes. In deep lakes, large volumes of deep water oxygen remineralize organic carbon produced in the photic zone. Lakes are most likely to go anoxic at

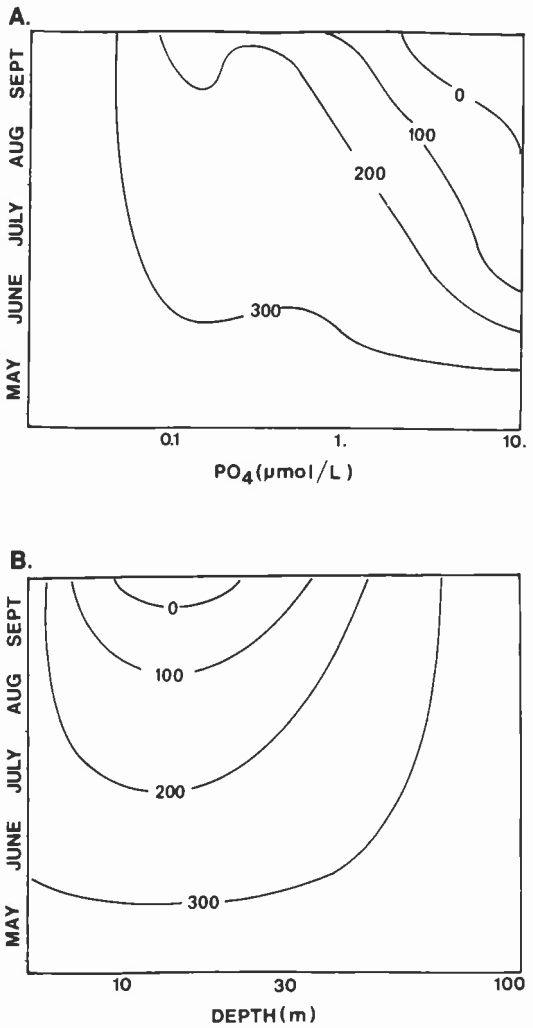

Figure 10.5. A. Initial average phosphate concentration versus time of model run. Contours are bottom water O_2 in μmole/L. B. Lake depth versus time of model run. Contours are bottom water O_2 in μmole/L.

Table 10.2
Summary of Sensitivity Analyses

Variable	Range Tested	Results
Lake depth	5–100 m	Anoxia most likely at intermediate depths
Initial PO_4 concentration	.01–10 μ mol/L	Anoxia most likely at high PO_4
Phytoplankton settling velocity	0.0–2.0 m/s	Little influence on anoxia between 1.0–2.0 m/s; <1.0 m/s causes oxygen depletion at intermediate depths
PO_4 half saturation constant	.01–.0001 μmol/L	Very little effect on the development of anoxia

Table 10.3
Lake characteristics and parameters used in model runs

	Esthwaite Water	Gem Lake
Location	English Lakes District 54°22′N, 0°49′W	Sierra Nevada, California 37°22′N, 118°45′W
Area	1 km^2	.03 km^2
Depth, maximum mean	15.5 m 6.4 m	7.0 m 3.4 m
Hydrodynamic features	Seasonal stratification, temperature gradient up to 12 °C	Variable but weak thermal stratification, temperature gradient of 0–2 °C
Initial model PO_4	2.0 μmole/L	0.2 μmole/L
Initial model POC	0.2 μmole/L	0.2 μmole/L
Maximum daily wind stress	0.4 dynes cm^{-2}	0.1 dynes cm^{-2}
Duration of model run	200 days	160 days
Phytoplankton settling velocity	1.0 ms^{-1} before June 30 0.3 ms^{-1} after June 30	1.0 ms^{-1}
Light half saturation constant	.001-ly^{-1} before June 30 .00027 ly s^{-1} after June 30	.001 ly s^{-1}
PO_4 half saturation constant	.002 μmol/L before June 30 .000025 μmol/L after June 30	.002 μmole/L

intermediate depth ranges (15–25 m for the conditions considered here). This depth range of anoxic bottom water would be considerably wider for higher average dissolved nutrient concentrations.

Sensitivity analyses of variables other than lake depth and initial PO_4 content were conducted. The results are summarized in table 10.2.

Application to Specific Lakes

The mathematical model described in appendix 10.1 has been applied to two lakes with widely varying chemical and biological properties. The areal size of the two lakes is small, however. This helps maintain the simplifications inherent in a 1-dimensional model. A summary of lake characteristics and modeling parameters is given in table 10.3.

Esthwaite Water

Esthwaite Water is a small biologically productive lake in the English Lakes district of northern England. The lake displays seasonal anoxia below a well-developed thermocline (Mortimer 1941, 1942; Sholkovitz and Copeland 1982). The lake also has a well-documented seasonal phytoplankton succession

(George and Heany 1978; Heany and Talling 1980). Diatoms are the dominant phytoplankton in the early spring. In the late spring and summer, the dinoflagellate *Ceratum hiumdimnella* and blue-green algae predominate. The dinoflagellates form cysts and disappear from the water column in the fall.

Wind stress to the Esthwaite Water simulations was set at a maximum of 0.35 dynes/cm^2. This roughly corresponds to the maximum daily wind speeds of 5–8 m/s reported in previous studies (Heany and Talling 1980). Maximum horizontal velocity at 0.5 m depth predicted by the model (14 cm/s) compares reasonably well with reported values of 9–11 cm/s (George and Heany 1978).

The model simulations for Esthwaite Water were run for a 250-day season (mid-March to early November). Surface temperature values were taken from Sholkovitz and Copeland (1982). Initial PO_4 was set at 2 μmole/L (with the assumption of a Redfield ratio for the NO_3 data of George and Heany [1978]). Two sets of biological parameters were used in the Esthwaite Water simulations. From mid-March until the end of June, settling velocity, nutrient half saturation constant, and light half saturation constant typical of diatoms were used (table 10.3). Diatoms are relatively large and have dense, siliceous tests. Diatom settling rates are therefore higher than those of most other phytoplankton types. Nutrient half saturation constants are higher for larger phytoplankton (Epply, Rogers, and McCarthy 1969) and light half saturation constants are generally lower (Parsons, Takahashi, and Hargrave 1984). After June 30, biological parameters typical of dinoflagellates were used. Dinoflagellates are smaller than diatoms and therefore have smaller settling velocities and nutrient half saturation constants (table 10.3).

Model runs show excellent reproduction of the Esthwaite temperature profile (figure 10.6). Rapid heating occurs in May and early June. The thermocline is well developed at 6–8 m depth during most of the summer. Over-

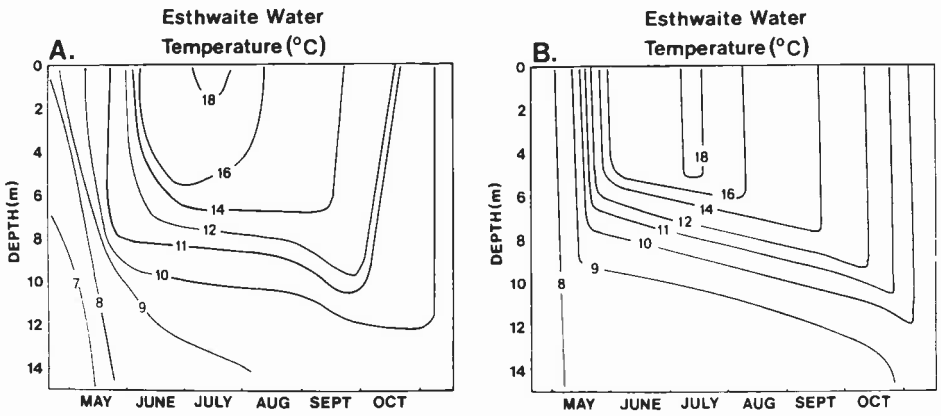

Figure 10.6. Time-versus-depth temperature profile for Esthwaite Water. A. Data of Sholkovitz and Copeland (1982). B. Model run. Contours are temperature in °C.

turning occurs in early November. The model deviates from the data by showing penetration of the 18°C isotherm somewhat deeper than the data indicate.

Oxygen profiles are also reasonably well predicted by the model (figure 10.7). Oxygen depletion begins to occur in the lower portion of the water column following the initiation of thermal stratification. This initial anoxia is believed to be the result of oxygen diffusion into the sediments (Sholkovitz and Copeland 1982). The model runs confirm this observation. Rapidly sinking diatoms (the dominant phytoplankton type) cause POC to build up in the sediments (equation 10A.19), which in turn leads to anoxia. The timescale of POC sinking from the photic zone (slightly less than 15 days) is somewhat less than the half-life of model POC below the photic zone (about 20 days; table 10.1). POC does not, therefore, remineralize prior to reaching the sediments.

Although most oxygen concentrations are well predicted by the model, the upward migration of completely anoxic water (defined by Sholkovitz and Copeland (1982) as $O_2 < 5$ μmole/L) is somewhat underpredicted. In the model, complete anoxia extends to 11 m depth whereas the data show anoxia at 8 m depth (figure 10.7). Other studies have indicated this depth varies between 8 and 10 m from year to year (Mortimer 1941, 1942). This discrepency can be explained by considering the diffusion length scale, l_d, in the hypolimnion:

$$l_d \equiv (K_h t)^{1/2} \tag{10.1}$$

In this equation K_h is eddy diffusivity and t is time. The model predicts that total diffusion (molecular plus eddy) is close to molecular diffusion (i.e., the order of 10^{-9} m^2/s) during thermal stratification. From the onset of bottom anoxia (mid-June) until seasonal overturn, l_d is approximately 3 m. This matches the limit of upward migration of anoxia predicted by the model (figure 10.7B). It also suggests that hypolimnion eddy diffusivities are being underpredicted by

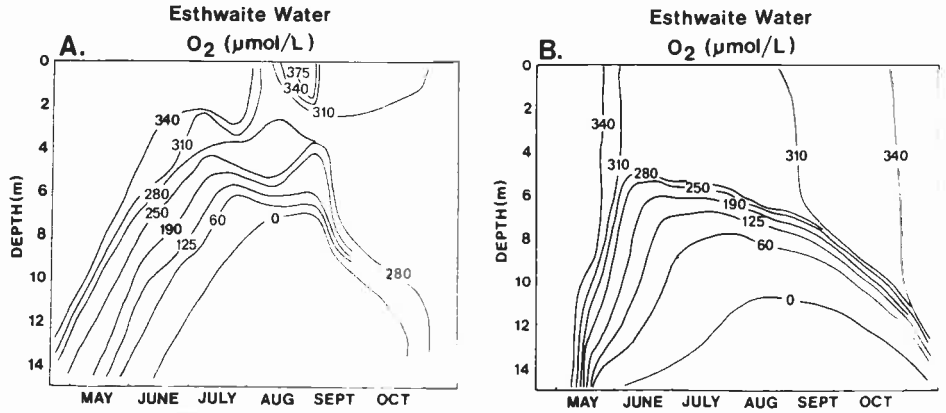

Figure 10.7. Time-versus-depth oxygen profile for Esthwaite Water. A. Data of Sholkovitz and Copeland (1982). B. Model run. Contours are O_2 in μmole/L.

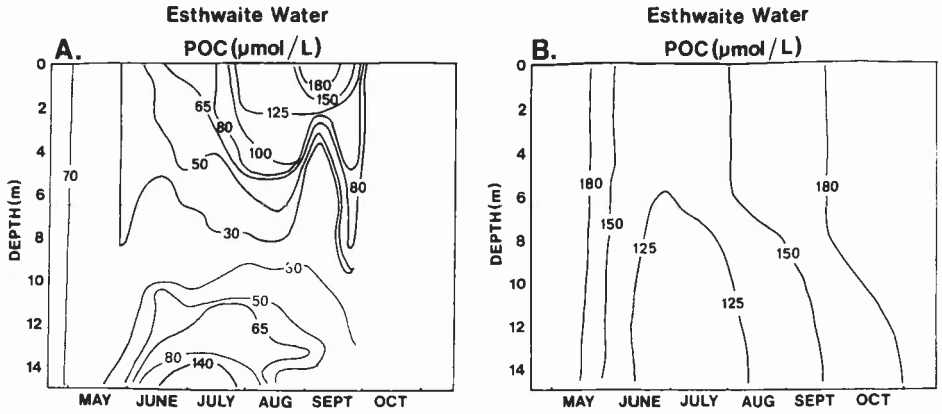

Figure 10.8. Time-versus-depth POC profile for Esthwaite Water. A. Data of Sholkovitz and Copeland (1982). B. Model run. Contours are POC in μmole/L.

the model and that they may be enhanced by a phenomenon such as internal waves.

Sholkovitz and Copeland (1982) show a period of surface oxygen supersaturation (up to 375 μmole/L) in late August that is not reproduced by the model. This may be the result of phytoplankton patchiness noted by previous researchers of Esthwaite Water (Heany and Talling 1980). This patchiness might cause short-term oxygen supersaturation.

POC is rather poorly predicted by the model (figure 10.8). Interpretation of POC data has shown the carbon cycle to be quite complex in Esthwaite Water (Sholkovitz and Copeland 1982). A spring diatom bloom causes uniform POC of 40–70 μmole/L (figure 10.8A). The model shows the bloom but gives POC values as much as three times higher. A deep water POC increase in midsummer is attributed to adsorption of dissolved organic carbon onto precipitating Fe-oxide particles (Sholkovitz and Copeland 1982). The model obviously does not account for this process; in fact the model shows a midsummer deep water POC minimum (figure 10.8B).

The model reproduces the midsummer dinoflagellate bloom, which causes surface POC to increase to 150–180 μmole/L (figure 10.8A, B). This bloom can logically be attributed to the dinoflagellate's ability to grow at lower nutrient levels (as shown by its smaller value of K_s (table 10.1)). This bloom can also be attributed to the increase in flux of nutrients to the surface following the seasonal temperature maximum that was observed in the generic model runs (figure 10.4).

Comparison of Esthwaite Water model results with the generic model run is instructive (figure 10.3). The onset of elevated POC concentrations and bottom water anoxia is much more rapid in Esthwaite Water, despite the fact that initial PO_4 and phytoplankton settling velocity are the same in both model runs. This phenomenon appears to be the result of different temperature inputs

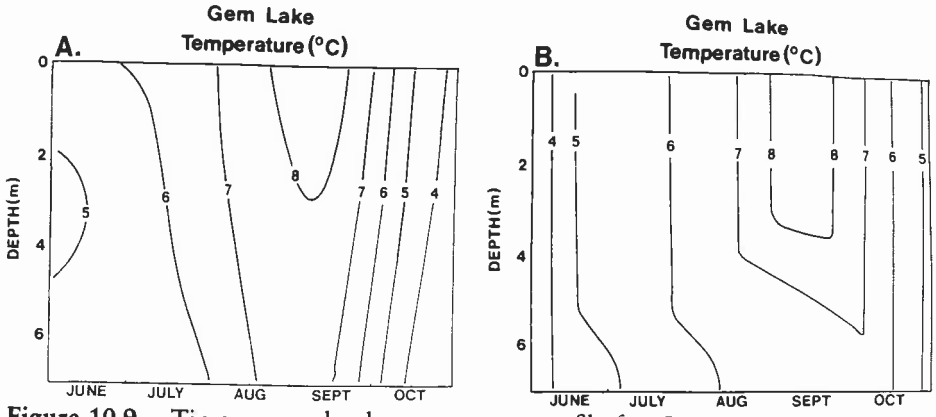

Figure 10.9. Time-versus-depth temperature profile for Gem Lake. A. Data of Stoddard (1987). B. Model run. Contours are in °C.

for the two situations. Thermal stratification exists from the outset of the generic model run, effectively cutting off diffusion of bottom water nutrients to the photic zone (figure 10.3B). The Esthwaite Water simulation is controlled by real surface temperature data; stratification does not become well established until early June (figure 10.6). Vertical mixing of nutrients prior to this time is very efficient and the spring bloom is more vigorous. Preliminary sensitivity analyses indicate that variable half saturation constants K_s and I_k (table 10.2) are not the cause of the observed differences in O_2 and POC.

Gem Lake

Gem Lake is a small, oligotrophic lake in the high Sierra Nevada of California. Lake elevation is 3300 m and the lake remains ice covered until early summer. The lake has relatively low dissolved nutrient concentrations. Oxygen depletion, while irregular on a seasonal basis, is usually minor. Trace metal nutrients may limit phytoplankton growth more severely than nitrogen or phosphorous (Stoddard 1986).

Gem Lake simulations were conducted for 160 days using the surface temperature and initial conditions of Stoddard (1986, 1987). The model used data of 1984, a year in which a complete spring-fall data set was available. No information is available on the phytoplankton type in Gem Lake. Biological parameters typical of diatoms were used (tables 10.1, 10.3), although sensitivity analyses have demonstrated that these parameters do not influence the simulations dramatically (table 10.2).

Reproduction of temperature profiles is good (figure 10.9). Thermal stratification of Gem Lake is very slight (top to bottom temperature gradient of 1.5°C in 1984). Model simulations indicate that thermal stratification is very sensitive to the amount of wind stress applied to such shallow lakes. The 1984

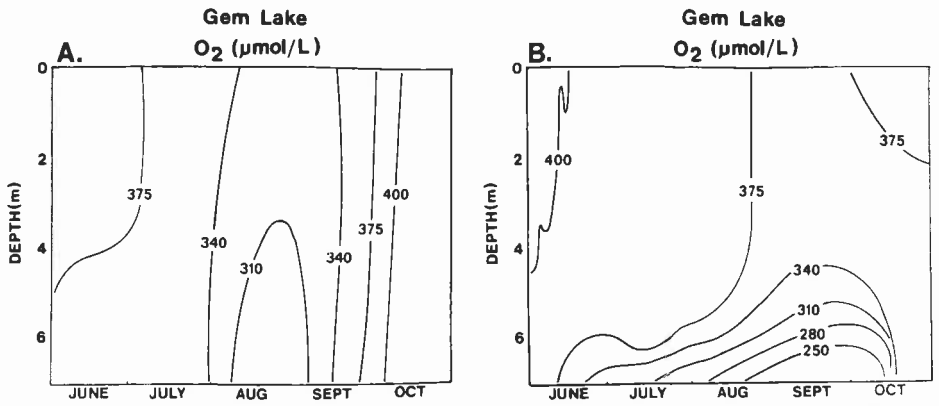

Figure 10.10. Time-versus-depth oxygen profile for Gem Lake. A. Data of Stoddard (1987). B. Model run. Contours are O_2 in μmole/L.

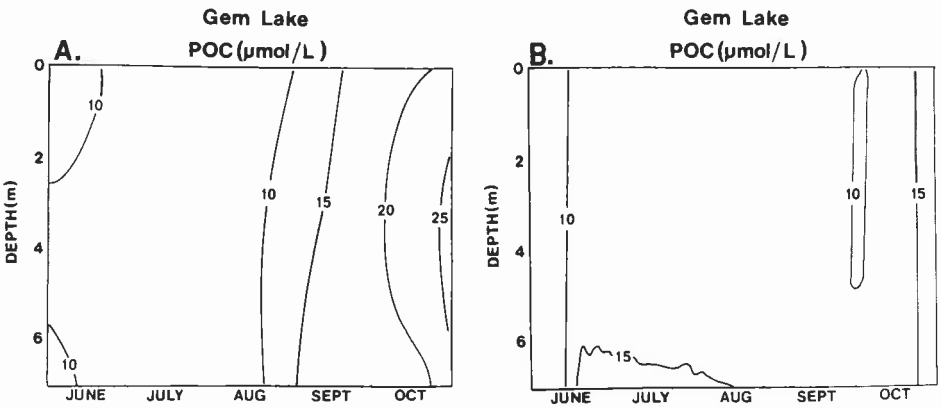

Figure 10.11. Time-versus-depth POC profile for Gem Lake. A. Data of Stoddard (1987). B. Model run. Contours are POC in μmole/L.

simulation was conducted at very low daily wind stress values (0.1 dynes/cm^2). Higher wind stress values (0.25 dynes/cm^2) caused complete thermal homogenization of the water column.

Oxygen and POC profiles were reasonably well predicted by the model (figures 10.10, 10.11). The model shows higher bottom water oxygen depletion than the data do (figure 10.10A, B). This could be due to overestimation of POC flux to the bottom (i.e., phytoplankton settling rate) by the model. Bottom POC is also overpredicted by the model (figure 10.11A, B). With the exception of bottom concentrations, predicted oxygen values are within 10% of the data, while POC values are within 30%.

Although bottom water oxygen depletion was minor in Gem Lake in 1984, it was virtually absent in 1982 and 1983 (Stoddard 1987, figure 10.5). This seasonal variability in oxygen concentrations might logically be explained by

variable wind shear stress. Although weather patterns over the lake are probably the same on a seasonal basis, summer storms may have thoroughly mixed the water column in some years but not others. Such variable mixing would be most likely to occur in shallow water bodies such as Gem Lake.

Discussion

A simple three-component geochemical model coupled to a sophisticated turbulence closure fluid dynamic model has a demonstrated ability to reproduce observed synoptic dissolved oxygen contents of water in shallow lakes. The model should be an effective tool for the study of oxygen fluxes in other modeling domains.

The model appears to overpredict particulate organic carbon, POC. Accurate prediction of POC probably must be done with more sophisticated ecological models than the one presented here. The overprediction in biologically active lakes is probably due to the fact that zooplankton grazing is not specifically modeled. Zooplankton fecal material tends to be rapidly transported out of the water column and into the sediment. Incorporation of a zooplankton component into the model will be a future improvement.

The model used in this study seems to be an effective tool for predicting bottom water anoxia. Oxygen is transported through the water column primarily by diffusion, whereas POC is transported by both diffusion and advection (i.e., particle settling). Eddy diffusivity is the quantity that the Mellor-Yamada turbulence closure scheme predicts very accurately; therefore, oxygen can be more accurately modeled. This appears to be particularly true for bottom water anoxia, which is a critical factor in organic carbon preservation.

The model demonstrates the importance that water depth has on the development of anoxia. Thermally stratified deep lakes have the ability to remain oxygenated by virtue of their deep water oxygen content. Very shallow lakes tend to stay oxygenated because of wind-induced shear stress. If all other conditions are constant, lakes of intermediate depth are the most likely to go anoxic during the summer. Elevated nutrient concentrations expand the depth range over which bottom water anoxia can occur. However, this generalization applies only to seasonally anoxic lakes. Permanently stratified lakes such as Lake Tanganyika or saline lakes would clearly not follow this pattern.

Examination of selected ancient lacustrine sediments in light of the results and qualifications given above is, however, interesting. Lacustrine depositional environments can be broadly classified into open basin and closed basin (Allen and Collinson 1986). The former includes freshwater lakes while the latter usually implies saline lakes, which are often permanently stratified.

In certain open basin lacustrine sequences, paleodepths have been estimated by a variety of techniques. Lakes with paleodepth estimates less than 100 m

Table 10.4
Summary of paleolimnology of selected open basin lacustrine sediments

Formation	Age	Anoxia	Max. Depth	Ref. and Notes
Culpeper Group, Virginia, USA	Jurassic	Yes	35 m	Hentz (1985). Deep water facies lacks bioturbation
East Berlin Formation, Connecticut, USA	Triassic	Yes	80 m	Hubert et al. (1976). Laminated black shale in deep water facies
Orcadian Basin, SE Scotland	Devonian	Yes	>10 m	Allen (1981a, b). Maximum depth not given, but lake believed to be less than 20 km wide
Karoo Basin, Natal, South Africa	Permo-Triassic	No	150 m	VanDijk et al. (1978)

generally have some sort of organic-rich facies or characteristics of anoxic bottom water (table 10.4) associated with them. On the other hand, Permo-Triassic sediments of the Karoo basin are hypothesized to have been deposited in a lake at least 150 m deep (table 10.4). Most of the Karoo sediments show evidence of benthic organisms, indicating that the bottom water was oxygenated.

These examples appear to fit the generalized model trend of lake bottom anoxia and lake depth (figure 10.5B), although it is certainly imprudent to extrapolate the results of this study to every open basin lacustrine setting. Future research will concentrate on combining more advanced models with detailed field studies. Plans are currently under way to expand the model to 2 or 3 dimensions and to include more sophisticated treatment of bottom sediment and organic carbon accumulation boundary conditions. These improvements should permit generalized patterns of organic facies to be constructed as a function of lake depth and shape. Future field studies of lacustrine sequences might easily be integrated into the modeling effort. For instance, if the formation of wave-induced sedimentary structures implies a given wind shear stress and/or lake depth, the model might predict whether anoxia may have been present above time-equivalent sediments elsewhere in the basin.

Appendix 10.1 Model Description

Equations of Motion

The mean velocity fields, U and V are described by the equations:

$$\frac{\partial U}{\partial t} = \frac{\partial}{\partial z}\left(-\overline{wu} + \nu_m \frac{\partial U}{\partial z}\right) \tag{10.1a}$$

$$\frac{\partial V}{\partial t} = \frac{\partial}{\partial z}\left(-\overline{wv} + \nu_m \frac{\partial V}{\partial z}\right) \tag{10.1b}$$

where $\overline{wu}$ and $\overline{wv}$ represent the turbulent Reynolds shear stress and ν_m is molecular kinematic viscosity. $-\overline{wu} \equiv K_m \partial U/\partial z$ and $-\overline{wv} \equiv K_m \partial V/\partial z$, where K_m is the eddy viscosity.

Conservation of heat is represented by:

$$\frac{\partial \Theta}{\partial t} = \frac{\partial}{\partial z}\left(\overline{-w\theta} + \nu_t \frac{\partial \Theta}{\partial z}\right) \tag{10.2}$$

where $\overline{w\theta}$ is the heat flux and ν_m is molecular thermal diffusivity. $\overline{w\theta} \equiv K_h \partial \Theta / \partial z$, where K_h is the eddy diffusivity.

Equations (10.1a, b,) and (10.2) do not include advection terms since horizontal velocities in lakes are small relative to their horizontal dimensions. Likewise, horizontal pressure gradients are considered small in lakes, and so pressure terms are not included in (10.1a, b) and (10.2).

The role of molecular effects in equations (10.1a, b) and (10.2) were examined in some detail during this study. In computer runs of a density-stratified water column with only modest wind shear, computed eddy viscosity and diffusivity values approached corresponding molecular values. When model runs were compared with synoptic temperature data sets, it was found that these molecular values did not transmit heat in a realistic fashion through the lower portion of the water column. This is consistent with published eddy diffusivity values, which are generally at least several times higher than molecular values.

This discrepancy can be explained by the inability of a 1-dimensional model to simulate 2- and 3-dimensional phenomena such as internal waves. In order to account for this shortcoming of the model, eddy viscosity and diffusivity were allowed to be no smaller than 5 times the corresponding molecular value. With this modification, the model gave accurate reproduction of temperature data. The change proved to be necessary only in the deeper portions of the model during periods of thermal stratification. Under all other circumstances, eddy values greatly exceeded molecular values.

The terms $\overline{wu}$, $\overline{wv}$, and $\overline{w\theta}$ in equations (10.1a, b) and (10.2) are solved on

the basis of the "Level 2-1/2" model of Mellor and Yamada (1982). Details of the 1-dimensional version of this model can be found in Mellor and Durbin (1975) and Weatherly and Martin (1978).

The balance between shear and buoyancy energy production can be more clearly seen by multiplying equations (10.1a) and (10.1b) by U and V, respectively and equation (10.2) by $-\beta gz$ (where β is the coefficient of thermal expansion and g is gravitational acceleration). If molecular effects are ignored and the chain rule is applied (Mellor and Durbin 1975), these equations can be rewritten as:

$$\frac{\partial}{\partial t}\left(\frac{U^2 + V^2}{2}\right) + \frac{\partial}{\partial_z}\left(U\overline{wu} + V\overline{wv}\right) = \overline{wu}\frac{\partial U}{\partial z} + \overline{wv}\frac{\partial V}{\partial z} \tag{10.3}$$

$$\frac{\partial}{\partial t}\left(-\beta gz\Theta\right) + \frac{\partial}{\partial z}\left(-\beta gz\overline{w\theta}\right) = -\beta g\overline{w\theta} \tag{10.4}$$

These equations represent balances of kinetic and potential energy. If one ignores the molecular effects (i.e., ν_m and ν_t) and integrates over depth, equation (10.3) and (10.4) can be rewritten in symbolic form as:

$$\frac{\partial}{\partial t}(KE) + W + SP = O \tag{10.5}$$

$$\frac{\partial}{\partial t}(PE) + BP = O \tag{10.6}$$

where KE = kinetic energy, W = surface wind stress work, SP = energy production by shear, PE = potential energy, and BP = buoyancy energy production (Mellor and Durbin 1975).

Geochemical Equations

Conservation of mass is represented by:

$$\frac{\partial C_i}{\partial t} + w_s\frac{\partial C_i}{\partial z} = \frac{\partial}{\partial z}\left(-\overline{wc_i} + \nu_c\frac{\partial C_i}{\partial z}\right) + (P - R)\,C_i \tag{10.7}$$

where C_i represents the concentration of the i-th chemical or biological component, P and R are production and loss rates, respectively, of C_i. The w_s represents vertical settling velocity for biogenic components and ν_c is molecular diffusivity for chemical components.

For the purpose of this work, P and R in equation 10.7 represent photosynthesis and respiration, respectively. Without bothering to rewrite advection and diffusion terms, equation 10.7 can be specified as coupled rate expressions for the three chemical components:

$$\frac{\partial O_2}{\partial t} = (P - R)\, POC \left[\frac{1}{r_{POC:O_2}}\right] \tag{10.8a}$$

$$\frac{\partial PO_4}{\partial t} = (R - P)\, POC \left[\frac{1}{r_{POC:PO_4}}\right] \tag{10.8b}$$

$$\frac{\partial POC}{\partial t} = (P - R)\, POC \tag{10.8c}$$

where $r_{POC:O2}$ and $r_{POC:PO4}$ are determined by the well-known Redfield ratio for algal material:

$$106CO_2 + 16NO_3^- + HPO_4^{2-} + 18H^+ + 122H_2O = 106(CH_2O)16(NH_3)(H_3PO_4) + 138O_2 \tag{10.9}$$

POC represents both living and dead algal material. Photosynthesis rates decrease exponentially with depth, thereby causing the POC component to produce oxygen in the photic zone while consuming it at depth. The use of one component to model all forms of organic carbon adds simplicity to the computations and allows the geochemical equations to be linear rather than nonlinear. This simplification also probably introduces the greatest error into the model. Zooplankton grazing and growth are specifically not included in this shallow lake model. Potential errors associated with this assumption are discussed above. For deep ocean models, a zooplankton component would have to be included, since it has long been recognized that zooplankton egesta play a critical role in the cycling of marine carbon (Parsons, Takahashi, and Hargrave 1984).

Various equations have been proposed to model photosynthesis. The most common models parameterize photosynthesis as an optimal growth rate factor, an exponential light intensity factor, and a hyperbolic nutrient limitation factor. Here we employ one such expression (Parsons, Takahashi, and Hargrave 1984):

$$P = P_{\max} \frac{I/I_k}{(1 + (I/I_k)^2)^{1/2}} \left(\frac{C_i}{K_s + C_i}\right) \tag{10.10}$$

where $P_{\max}$ is maximum growth rate, I is light intensity, I_k the saturation constant for light limitation of phytoplankton growth, and K_s the half saturation constant for a particular nutrient involved in the phytoplankton growth. The limiting nutrient in this study is phosphate, which has been shown to be the limiting nutrient in most natural lakes (Schindler 1974).

Maximum phytoplankton growth is modeled with the temperature-dependent function:

$$P_{\max} = .59e^{.0633\,T} \tag{10.11}$$

where T is temperature in degrees centigrade. This relationship appears to be valid for a wide variety of phytoplankton types under a variety of environmental conditions (Epply 1972; Goldman and Carpenter 1974).

Light intensity attenuation with depth is modeled according to the relationship given by Parsons, Takahashi, and Hargrave (1984).

$$I = I_o e^{-kd} \tag{10.12}$$

where I_o is light intensity at the surface, d is depth, and k is the light extinction coefficient.

I_o varies according to season and time of the day. Seasonal variation was determined as a sine wave with maximum and minimum taken from standard tables for a given latitude (e.g., Smithsonian Meteorological Tables 1951). Daily light intensity was calculated according to a half sine wave from 0600–1800 hours. No seasonal variation in day length was added to the model.

The model uses the following expression, which relates the light extinction coefficient to concentration of phytoplankton in water (Riley 1956):

$$k = .04 + .0088chl - a + .054(Chl - a)^{2/3} \tag{10.13}$$

The first term in equation (10.13) is the extinction coefficient for pure water while the second and third terms account for shading by phytoplankton. Chl-a represents concentration of chlorophyll a in $\mu g/L$. Chl-a is converted to POC by the model with average conversion factors (Parsons, Takahashi, and Hargrave 1984).

Respiration of organic matter (R in equations (10.7) and (10.8)) and subsequent uptake of oxygen have been determined experimentally and empirically in a number of aqueous environments. In general, respiration follows a Michaelis-Menten equation similar to that used to model photosynthesis (Berner 1980):

$$R = R_{\max}\left(\frac{O_2}{Ks_{O_2} + O_2}\right) \tag{10.14}$$

For this study, $R_{\max}$ is set to equal the value of fresh phytoplankton. Values of Ks_{O_2}, the half saturation constant for oxygen, are not readily available in the literature. $Ks_{O_2} = 100$ μmole O_2 is, however, a value that appears to approximate respiration rate data in other natural waters (e.g., Emerson 1985). Equations (10.1a, b), (10.2), and (10.7) were solved with an implicit finite difference scheme. Most computer runs used 40 grid points with logarithmic spacings at the top and bottom of the domain. The time step was set at 30 minutes. One-year model simulations take approximately 1 minute of CPU time on a CYBER-205 supercomputer.

Boundary Conditions

At the surface, temperature is specified for all modeling runs:

$$\Theta(O,t) = \Theta_s\,(t) \tag{10.15}$$

For specific lakes described below, the surface temperatures are taken from data sets in published literature. For the generalized lake models described below, surface temperature input is derived from a seasonally varying half sine function. At the bottom, zero temperature gradient is specified so that:

$$\Theta(z_n,t) = \Theta(z_{n-1},t - 1) \tag{10.16}$$

where z_0, z_1, . . . z_{n-1}, z_n refer to grid points in the modeling domain from top to bottom.

Surface wind stress represents the only kinetic energy input to the model, and therefore is the only factor to influence the depth of the thermocline. For this study, surface wind stress is specified as a daily sine function:

$$(-\overline{wu},\ -\overline{wv})\ z = 0 = A\left(sin\ \frac{2\pi t}{T},\ sin\ \frac{2\pi t}{T}\right) \tag{10.17}$$

where T is 1 day and A is maximum daily wind stress. Note that equations (10.1a, b) and (10.2) do not have a steady state solution. The use of a periodic boundary condition (10.17) keeps horizontal velocity solutions within a specified range. For the models of specific lakes described above, the magnitude of wind stress was increased until the depth of the thermocline matched that of the temperature data. At the base of the modeling domain, bottom shear stress was set by matching bottom velocities to the logarithmic law of the wall.

Oxygen in the uppermost layer of the model is set at the saturation level for a given temperature according to the polynomial expression of Carpenter (1966).

At each time step of the model, the surface flux was zero so that surface concentrations of PO_4 and POC were set to match concentrations at the closest interior grid point. At the bottom grid point, particulate organic carbon accumulates according to the expression:

$$F = w_s\ POC\ (z_{n-1},t - 1) \tag{10.18}$$

where F is flux of POC in μmol dm^{-2}/s. Bottom O_2 and PO_4 concentrations are then set according to the rate expressions of equations (10.8a) and (10.8b). At each time step, a mass balance is performed on PO_4 to ensure that the total amount of particulate and dissolved phosphate in the modeling domain remains constant.

Glossary of Terms

Buoyancy energy production—energy produced by vertical density gradients in a fluid. Abbreviated as BP, it is decreased by solar heating or freshwater input at the surface.

Eddy diffusivity—diffusivity of a fluid, which is produced by fluid turbulence. The more turbulent the fluid, the greater the eddy diffusivity and, hence, the fluid mixing.

Eddy viscosity—viscosity of a fluid, which is produced by fluid turbulence. The more turbulent the fluid, the greater the eddy viscosity.

Epilimnion—the relatively warm, well-mixed surface water of a lake, which is in contact with the atmosphere.

Hypolimnion—the relatively cold, poorly mixed deep water of a lake, which is in contact with the sediments.

Internal waves—moving, horizontal variations in fluid density. Internal waves can enhance fluid mixing.

Michaelis-Menten kinetics—the use of a hyperbolic function to describe the change in photosynthesis with changing limiting nutrient content.

Redfield ratio—the average molecular ratios of carbon, nitrogen, phosphorous in algae.

shear energy production—energy produced by velocity gradients in a fluid. Abbreviated as SP, it is generally caused by winds in lakes.

thermocline—the zone of maximum temperature gradient in a water column.

Acknowledgments

Computing time for this research was provided by the Program in Atmospheric and Oceanic Sciences, Princeton University, and the Geophysical Fluid Dynamics Laboratory, National Oceanic and Atmospheric Administration. Discussions with George Mellor and Bob Stallard guided the modeling effort. The manuscript benefited from reviews by Jorge Sarmiento, Ray Najjar, George Mellor, Jean Whelan, Eileen Hofmann, and David Glover.

References

Allen, P. A. 1981a. Devonian lake margin and processes, SE Scotland: *J. Geol. Soc. Lond.* 138:1–14.

Allen, P. A. 1981b. Wave generated structures in the Devonian lacustrine sediments of southeast Shetland and ancient wave conditions. *Sedimentol.* 28:369–379.

Allen, P. A. and J. D. Collinson. 1986. Lakes. In H. G. Reading ed., *Sedimentary Environments and Facies*, pp. 63–94. Oxford: Blackwell.

Batchelor, G. K. 1967. *An Introduction to Fluid Dynamics*. Cambridge: Cambridge University Press.

Berner, R. A. 1980. Early diagenesis. Princeton, N.J.: Princeton Univ. Press.

Blatt, H., G. Middleton, and R. Murray. 1980. Origin of sedimentary rocks. Englewood Cliffs, N.J.: Prentice Hall.

Broecker, W. S. and T. H. Peng. 1982. Tracers in the sea. Palisades, N.Y.: Eldigo.

Carpenter, J. H. 1966. New measurements of oxygen solubility in pure and natural water. *Limnol. Oceangr.* 11:264–277.

Chemical Rubber Company (CRC). 1977. *Handbook of Chemistry and Physics*. Cleveland, Ohio: Chemical Rubber Company Press.

Demaison, G. J. and G. T. Moore. 1980. Anoxic environments and oil source bed genesis. *Am. Assoc. Petrol. Geol. Bull.* 64:1179–1209.

Emerson, S. 1985. Organic carbon preservation in marine sediments. In E. T. Sundquist and

W. S. Broecker, eds., *The Carbon Cycle and Atmospheric* CO_2: Natural Variations Archean to Present, pp. 78–88. Washington, D.C.: Am. Geophys. Union Geophys. Monograph series, vol. 32.

Epply, R. W. 1972. Temperature and phytoplankton growth in the sea. *Fish Bull.* 70:1063–1085.

Epply, R. W., J. N. Rogers, and J. J. McCarthy. 1969. Half saturation constants for uptake of nitrate and ammonium by marine phytoplankton. *Limnol. Oceanogr.* 14:912–920.

Gachter, R. and D. M. Imboden. 1985. Lake restoration. In W. Stumm, ed., *Chemical Process in Lakes*, pp. 363–388. New York: Wiley.

George, D. G. and S. I. Heany. 1978. Factors influencing spatial distribution of phytoplankton in a small productive lake. *J. Ecol.* 66:133–155.

Goldman, J. C. and E. J. Carpenter. 1974. A kinetic approach to the effect of temperature on algal growth. *Limnol. Oceangr.* 19:756–766.

Hanton, J. T. 1969. Algal phosphate uptake, kinetic growth rates and limiting phosphate concentrations. M. S. thesis, Univ. of North Carolina, Chapel Hill, N.C.

Heany, S. I. and J. F. Talling. 1980. Dynamic aspects of dinoflaggelate distribution patterns in a small productive lake. *J. Ecol.* 68:75–94.

Hentz, T. F. 1985. Early Jurassic sedimentation of a rift-valley lake: Culpepper basin, northern Virginia. *Geol. Soc. Am. Bull.* 96:92–107.

Higgins, J. M. and B. R. Kim. 1982. DO model for discharge from deep impoundments. *Proc. ASCE, J. Env. Eng. Div.* 108 (EE1):107–122.

Hofmann, E. E. 1988. Plankton dynamics on the outer southeastern U. S. continental shelf. III. A coupled physical-biological model. *J. Mar. Res.* 46:919–946.

Hofmann, E. E. and J. W. Ambler. 1988. Plankton dynamics on the outer southeastern U. S. continental shelf. II. A time dependent biological model. *J. Mar. Res.* 46:883–917.

Hubert, J. F., A. A. Reed, P. J. Carey. 1976. Paleogeography of the East Berlin Formation, Newark Group, Connecticut Valley. *Am. J. Sci.* 276:1183–1207.

Jamart, B. M., D. F. Winter, K. Bause, G. C. Anderson, and R. K. Lam. 1977. A theoretical study of phytoplankton growth and nutrient distribution in the Pacific Ocean off the northwestern U. S. coast. *Deep Sea Res.* 24:753–773.

Kremer, J. N. and S. W. Nixon. 1978. A coastal marine ecosystem. Berlin: Springer Verlag.

Li, Y.-H. and S. Gregory. 1974. Diffusion of ions in seawater and in deep sea sediments. *Geoch. Cosmochim. Acta* 38:703–714.

Mellor, G. L. and P. A. Durbin. 1975. The structure and dynamics of the ocean surface mixed layer. *J. Phys. Oceanogr.* 5:718–728.

Mellor, G. L. and T. Yamada. 1974. A hierarchy of turbulence closure models for planetary boundary layers. *J. Atmos. Sci.* 31:1791–1806.

Mellor, G. L. and T. Yamada. 1982. Development of turbulence closure models for geophysical fluid dynamics problems. *Rev. Geophys. Space Phys.* 20:851–875.

Mortimer, C. H. 1941. The exchange of dissolved substances between mud and water in lakes, parts I, II. *J. Ecol.* 29:280–329.

Mortimer, C. H. 1942. The exchange of dissolved substances between mud and water in lakes, parts III, IV. *J. Ecol.* 30:147–201.

Oey, L.-Y., G. L. Mellor, and R. I. Hires. 1985. A three-dimensional simulation of the Hudson-Raritan estuary. Part I. Description of the model and model simulations. *J. Phys. Oceangr.* 15:1676–1692.

Parsons, T. R., M. Takahashi, and B. Hargrave. 1984. *Biological Oceanographic Processes.* New York: Pergamon Press.

Quay, P. D., W. S. Broecker, R. H. Hesslein, and D. W. Schindler. 1980. Vertical diffusion rates determined by tritium tracer experiments in the thermocline and hypolimnion of two lakes. *Limnol. Oceangr.* 25:201–218.

Riley, G. A. 1956. Oceangraphy of Long Island Sound, 1952–1954. IX. Production and utilization of organic matter. *Bull. Bingham Oceangr. Coll.* 15:324–343.

Sarmiento, J. L., T. D. Herbert, and J. R. Toggweiler. 1988a. Causes of anoxia in the world ocean. *Global Biogeochem. Cycles* 2:115–128.

Sarmiento, J. L., T. D. Herbert, and J. R. Toggweiler. 1988b. Mediterranean nutrient balance and episodes of anoxia. *Global Biogeochem. Cycles* 2:427–444.

Schindler, D. W. 1974. Eutrophication and recovery in experimental lakes: implications for lake recovery. *Science* 184:897–899.

Shaffer, G. 1989. A model of biogeochemical cycling of phosphorous, nitrogen, oxygen, and sulfur in the ocean: one step toward a global climate model. *J. Geophys. Res.* 94:1979–2004.

Sholkovitz, E. R. and D. Copeland. 1982. The chemistry of suspended matter in Esthwaite Water, a biologically productive lake with seasonally anoxic hypolimnion. *Geochim. Cosmochim. Acta* 46:46,393–410.

Smayda, T. J. 1970. The suspension and sinking of phytoplankton in the sea. *Oceangr. Mar. Biol. Ann. Rev.* 8:353–414.

Smithsonian Meterological Tables. 1951. Publication 4014. Washington, D.C.: The Smithsonian Institution.

Snodgrass, W. J. and C. R. O'Melia. 1975. Predictive model for phosphorous in lakes. *Environ. Sci. Technol.* 9:937–944.

Southam, J. R. and W. H. Peterson. 1985. Transient response of the marine carbon cycle. In E. T. Sundquist and W. S. Broeker, eds., *The Carbon Cycle and Atmospheric* CO_2: Natural Variations Archean to Present, pp. 89–98. Am. Geophys. Union Geophys. Monograph series, v. 32, Washington, D.C.: Am. Geophys. Union.

Stoddard, J. L. 1986. Nutritional status, microcrustacean communities, and susceptibility to acid precipitation of high elevation lakes in the Sierra Nevada, California. Ph.D. thesis, Univ. Calif., Santa Barbara.

Stoddard, J. L. 1987. Alkalinity dynamics in an unacidified alpine lake, Sierra Nevada, California. *Limnol. Oceangr.* 32:825–839.

VanDijk, D. E., D. K. Hobday, and A. J. Tankard. 1978. Permo-Triassic lacustrine deposits in the eastern Karoo Basin, Natal, South Africa. In A. Matter and M. E. Tucker, eds., *Modern and Ancient Lake Sediments*, pp. 223–238. Int. Assoc. Sedimentologists, spec. publ. 2.

Vollenweider, R. A. 1975. Input-output models. *Schwiez. Z. Hydrol.* 37:53–84.

Walsh, J. J. 1975. A spatial simulation of the Peruvian upwelling ecosystem. *Deep Sea Res.* 22:201–236.

Weatherly, G. and P. J. Martin. 1978. On the nature and dynamics of the ocean bottom boundary layer. *J. Phys. Oceangr.* 8:557–570.

Westrich, J. T. and R. A. Berner. 1984. The role of sedimentary organic matter in bacterial sulfate reduction: the G-model tested. *Limnol. Oceangraph* 29(2):236–249.

Wroblewski, J. S. 1977. A model of phytoplankton plume formation during variable Oregon upwelling. *J. Mar. Res.* 35:357–394.